ADVANCED OPTICAL MATERIALS
www.advopticalmat.de

Optical Polarization Encoding Using Graphene-Loaded Plasmonic Metasurfaces

Jianxiong Li, Ping Yu, Hua Cheng, Wenwei Liu, Zhancheng Li, Boyang Xie, Shuqi Chen, and Jianguo Tian**

Plasmonic metasurfaces are a new class of quasi 2D metamaterials that provide fascinating capabilities for manipulating light in an ultrathin platform.[1] By engineering the geometry of nanostructured metasurfaces, the spectral and spatial dispersion of their optical responses can be tailored across the electromagnetic spectrum.[2–5] Some exotic phenomena have been demonstrated using plasmonic metasurfaces, including anomalous reflection and refraction,[6–10] the spin-Hall effect of light,[11] perfect absorbance,[12–14] and optical polarization conversion of light.[15–17] Hyperbolic metasurfaces also provide high degree of freedom to steer the polarization of surface wave.[18] Recently, the research focus has shifted toward achieving tunable and switchable metasurfaces.[19,20] This transformation from metasurfaces to metadevices is highly desirable and can potentially expand the range of their applications. Moreover, a large number of traditional optical devices have been miniaturized and integrated, such as spatial light modulators, optical switches, and optoelectronic devices, and a number of dynamical tuning methods based on thermal, mechanical have been reported.[21–23] However, these methods are usually limited by slow switching speeds or small tunable ranges.

Graphene is a monolayer of hexagonally arranged carbon atoms, and its optical conductivity and permittivity show a strong dependence on the Fermi level, which can be dynamically controlled by a gate voltage.[24–26] Therefore, graphene is a promising electrically tunable material. The combination of metasurfaces and graphene is emerging as a possible platform for electrically controlled plasmonic devices with high response speeds due to the enhanced graphene–light interaction. Thus, the characteristics of graphene-loaded plasmonic metasurfaces could fulfill the ever-increasing demand for faster information transfer and processing, parallel data processing, and compact space operations. The fulfillment of these increasing demands requires control of the electromagnetic properties of matter through external stimuli such as electric signals. The electrically controllable optical response of plasmonic metasurfaces with graphene has been shown at the near-infrared (NIR), mid-infrared (MIR)[27–29] and terahertz wavelengths.[30,31] In particular, plasmonic metasurfaces with graphene can be used as optical switches by dynamically tuning the light amplitude to realize amplitude encoding in modern optical communication devices.[32,33]

Moreover, the development of a feasible metadevice design that has the ability to dynamically tune the light polarization state has attracted enormous interest. Such metadevices can be employed for realizing not only the polarization encoding but also polarization-division multiplexing (PDM), which is a crucial technique that can significantly increase the transmission capacity of a single physical channel.[34] The traditional technique for realizing PDM requires a complex optical system and cumbersome volume. Therefore, a metadevice-based polarization modulator offers a new approach for simplifying the optical process and miniaturizing the required volume. Although metasurfaces can transform light polarization, the change of polarization-control characteristic requires variation of the size, shape, and material properties of the structure. Hence, the dynamical manipulation of the polarization state using a metasurface is still challenging.

In this work, we propose a metadevice by integrating a single layer of graphene with an anisotropic metasurface, which can dynamically modulate the polarization state of light with wide tunable range in MIR wavelengths. By switching gate voltage applied on the graphene among three different values, the incident linearly polarized (LP) light can be dynamically converted into left circularly polarized (LCP) light, right circularly polarized (RCP) light, or linearly cross-polarized light in the reflection direction by the proposed metadevice. A continuous polarization evolution from LCP to RCP light can be achieved as the gate voltage gradually increases. In addition, two mutually perpendicular LP light beams and an elliptically polarized (EP) light beam can also be generated in the reflection direction by the proposed metadevice under EP light illumination. Based on these polarization-control characteristics, the proposed metadevice can realize polarization encoding and the PDM technique. The process of multiplexing and demultiplexing in the PDM technique can be accomplished by metadevices with a more simple approach and in a more compact space than traditional PDM techniques. The new degrees of freedom enabled by the metadevice facilitate the arbitrary manipulation of light polarization states and will profoundly affect a wide range of modern optical communication devices.

Control of the light polarization state is an important area of research for metasurfaces. The anisotropy of plasmonic metasurfaces plays a dominant role in manipulating the light polarization state. The different optical responses along two orthogonal principal axes of the nanostructures result in different amplitude attenuation and phase retardation of the

Dr. J. Li, Dr. P. Yu, Prof. H. Cheng,
Dr. W. Liu, Dr. Z. Li, Dr. B. Xie,
Prof. S. Chen, Prof. J. Tian
Laboratory of Weak Light Nonlinear Photonics
Ministry of Education
School of Physics and Teda Applied Physics Institute
Nankai University
Tianjin 300071, China
E-mail: schen@nankai.edu.cn; jjtian@nankai.edu.cn

DOI: 10.1002/adom.201500398

incident light.[35] By carefully engineering the geometrical parameters and the asymmetry of the nanostructures, the polarization state of light can be easily controlled. Considering incident light with certain polarization, the transmission or reflection process can be easily interpreted as

$$\begin{bmatrix} E_x \\ E_y \end{bmatrix} = \hat{P}\begin{bmatrix} \cos\theta \\ \sin\theta \end{bmatrix} = \begin{bmatrix} r_{xy}e^{-i\delta} & 0 \\ 0 & 1 \end{bmatrix}\begin{bmatrix} \cos\theta e^{-i\delta'} \\ \sin\theta \end{bmatrix} = \begin{bmatrix} r_{xy}e^{-i(\delta+\delta')}\cos\theta \\ \sin\theta \end{bmatrix} \quad (1)$$

where θ and δ' are the polarization direction and phase difference of incident light, respectively, and r_{xy} and δ are the amplitude attenuation ratio and phase retardation difference between two orthogonal E-field components caused by the metasurfaces, respectively. Therefore, the arbitrary polarization state of light can be achieved by tuning r_{xy} and δ while maintaining the polarization state of incident light. The metasurface-based quarter waveplates, which possess a 90° or 270° phase retardation difference with designed amplitude ratio r_{xy}, transform the linearly polarized incident light into RCP light or LCP light,[35–37] respectively. Similarly, metasurface-based half waveplates can achieve a complete cross-polarization conversion due to the $\delta = 180°$ phase retardation difference caused by the nanostructure.[38,39] Therefore, to dynamically modulate the polarization state of light, a hybrid structure consisting of plasmonic metasurfaces and a tunable material is required for actively adjusting the anisotropic optical responses (r_{xy} and δ). Graphene, a novel electrically controlled active medium, is an ideal material for satisfying this requirement due to its remarkable properties when the graphene interacts with metasurfaces.

The reasoning for dynamically modulating the polarization state by the graphene-loaded plasmonic metasurface can be explained as follows. First, the carrier density of graphene can be adjusted over a wide range at room temperature using the bias voltage, leading to a large change in conductivity σ in the MIR region.[40] Then, the electric permittivity $\varepsilon = 1 + i\sigma/(\varepsilon_0\omega t)$ can be widely modulated, where ε_0 is the vacuum permittivity, ω is the angular frequency, and t is the thickness of graphene. Second, when the graphene is deposed in hot spots created by metasurface, the electrically controllable electric permittivity of graphene can lead to wide tuning of the resonant frequency ω_{res} of the metasurface, i.e., tuning of the amplitude attenuation and phase retardation of light. According to perturbation theory, the change of ω_{res} caused by graphene is given by[41]

$$\frac{\Delta\omega_{\text{res}}}{\omega_o} = \frac{\omega_{\text{res}} - \omega_o}{\omega_o} \approx \frac{-\iiint dV\left[\left(\Delta\vec{\mu}\cdot\vec{H}\right)\cdot\vec{H}_o^* + \left(\Delta\vec{\varepsilon}\cdot\vec{E}\right)\cdot\vec{E}_o^*\right]}{\iiint dV\left(\mu\left|\vec{H}_o\right|^2 + \varepsilon\left|\vec{E}_o\right|^2\right)}. \quad (2)$$

Here, $\Delta\vec{\mu}$ and $\Delta\vec{\varepsilon}$, which are the changes of the magnetic permeability and electric permittivity of graphene, respectively, are regarded as the material perturbation. Moreover, ω_0 is the resonant frequency of the unperturbed metasurface, and $\vec{E}$ and $\vec{H}$ are electric and magnetic fields in the presence of perturbation, respectively. The unperturbed fields are given by $\vec{E}_0$ and $\vec{H}_0$, whose complex conjugates are represented by $\vec{E}_0^*$ and $\vec{H}_0^*$. The change in resonant frequency $\Delta\omega_{\text{res}}$, which determines the modulation ranges of the amplitude attenuation and phase retardation, is proportional to $\Delta\vec{\varepsilon}\cdot\vec{E}$. Thus, the value of $\Delta\omega_{\text{res}}$ relies on not only the material perturbation caused by graphene ($\Delta\vec{\varepsilon}$) but also the local enhancement of optical fields generated by the metasurface ($\vec{E}$).[42] By generating different local optical field intensities under the excitation with two orthogonal electrical directions, an anisotropic metasurface can achieve different tunable ranges of light amplitude attenuation and phase retardation along these two directions, even with the same $\Delta\vec{\varepsilon}$. Therefore, the remarkable characteristics of graphene-loaded metasurface can flexibly modulate the attenuation ratio r_{xy} and phase retardation difference δ, realizing dynamically tunable polarization states of light.

Figure 1a illustrates the schematic unit cell of the proposed electrically tunable hybrid plasmonic metasurfaces. It contains a gold film with a rectangular aperture and a gold substrate, which are separated by a SiO_2 layer, which has a dielectric constant of 2.25. The graphene sheet covers the entire SiO_2 layer. Rectangular aperture nanostructure has strong anisotropy, and it has largely different optical responses illuminated by the incident light polarized parallelly and vertically to the principal axis of rectangular aperture. The different optical responses along two orthogonal principal axes of the nanostructures result in different amplitude attenuation and phase retardation of the incident light. Meanwhile, due to the coupling between the nanostructure and the ground plane, the reflect-array with thick ground plane has the largest resonant wavelength shift as tuning the gate voltage applied on graphene.[42] The tunable hybrid plasmonic metasurfaces were designed and optimized with the finite element method-based COMSOL Multiphysics software.[43] The port boundary condition is employed to simulate the plane wave incidence normally to the structure. Perfectly matched layers are used at the top and bottom of the simulation domain to completely absorb waves, leaving the simulation domain in the direction of propagation. Periodic boundary conditions are used in the x and y directions. Graphene was modeled using one layer of mesh cells with thickness $t = 0.33$ nm, and the mesh size in the plane of graphene is 1 nm × 1 nm. The optical constants of gold in the infrared spectral regime are described using the Drude model.[44] Graphene layer is regarded as an anisotropic material with in-plane conductivity $\sigma_{\parallel}$ and out-of-plane permittivity $\varepsilon_{\perp}$. This method mainly focuses on the material effect in 2D flat surface while ignoring that in out-of-plane direction, which can simulate a 2D current in the graphene layer under the local electrical field. The out-of-plane dielectric constant of graphene remains at 2.25, which is the permittivity of substrate material and has tiny effects in the simulation results due to the thinness of graphene. The in-plane conductivity of graphene is calculated within the local random phase approximation:[45]

$$\sigma(\omega) = \frac{2ie^2k_BT}{\pi\hbar^2(\omega + i\tau^{-1})}\ln\left[2\cosh\left(\frac{E_f}{2k_BT}\right)\right] + \frac{e^2}{4\hbar}\left\{\frac{1}{2} + \frac{1}{\pi}\arctan\left(\frac{\hbar\omega - 2E_f}{2k_BT}\right) - \frac{i}{2\pi}\ln\left[\frac{(\hbar\omega + 2E_f)^2}{(\hbar\omega - 2E_f)^2 + (2k_BT)^2}\right]\right\} \quad (3)$$

Here, e is the elementary charge, k_B is the Boltzmann constant, $\hbar$ is the reduced Planck constant, and the temperature T is 300 K. Moreover, τ is the carrier relaxation lifetime at 0.25 ps,

Adv. Optical Mater. 2015,
DOI: 10.1002/adom.201500398

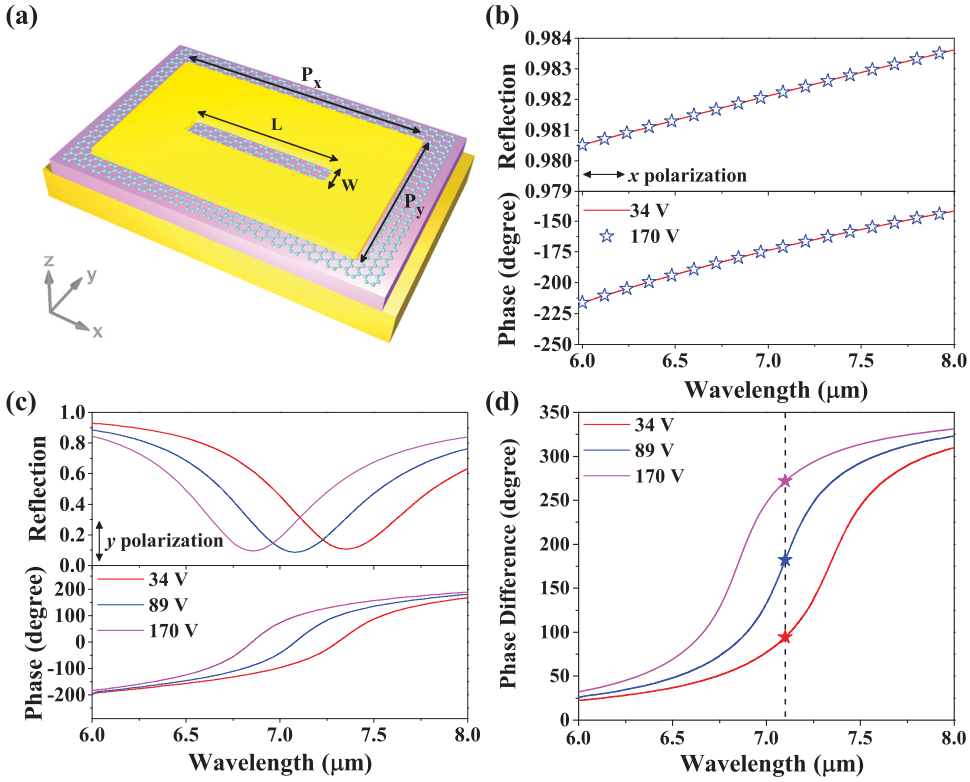

Figure 1. a) Schematic of the graphene-loaded plasmonic metasurface unit cell consisting of a 50-nm-thick gold film with a rectangular aperture and a 100-nm-thick gold substrate, which are separated by a 285-nm-thick SiO_2 layer. The graphene sheet covers the entire SiO_2 layer. The period of the unit cell in the *x* and *y* directions is P_x = 4.4 μm and P_y = 1.7 μm, respectively. The length and width of the rectangular aperture is L = 3.7 μm and W = 50 nm, respectively. b,c) Simulated amplitude and phase spectra of the reflection light from the nanoaperture array at different gate voltages illuminated with *x*- and *y*-polarized incident light, respectively. d) Phase retardation difference δ between incident light with *x*- and *y*-polarization as a function of the wavelength at different gate voltages. The stars indicate values of δ under different gate voltages at 7.1 μm.

and the carrier scattering rate is $1/\tau = 4\,\mathrm{THz}$, which is achievable in graphene with reasonably high carrier mobility.[46] Finally, $E_f = \hbar V_f \sqrt{\pi n_s}$ is the Fermi level, where $V_f = 10^6$ m s^{-1} is the Fermi velocity and n_s is the carrier density of graphene sheet. In practice, the carrier density of graphene n_s can be changed by applying a bias voltage. The carrier density of graphene sheet can be estimated as $n_s = a_c |V_G - V_{CNP}|$ by using the parallel capacitor model, where V_G is the gate voltage, and V_{CNP} is the voltage shifting the graphene Fermi level to the Dirac point. For a high-quality graphene monolayer, V_{CNP} is zero, and zero bias doping is also zero. $a_c = \frac{\varepsilon_r}{4\pi k_e d e}$ is the capacitor constant, where k_e is the electrostatic constant and e is the elementary charge. In our case, the relative permittivity of SiO_2 is ε_r = 2.25, and the separation d is 285 nm. The calculated capacitor constant a_c is 4.4×10^{14} m^{-2} V^{-1}.

The designed metadevice works in the reflection mode as the gold plane suppresses the transmission. The amplitude and phase spectra of reflection under incident light polarized in the *x*- and *y*-directions are shown in Figure 1b,c, respectively. There is no observed variation in the reflection and phase when the carrier density of graphene sheet is significantly changed from 1.5×10^{16} m^{-2} to 7.5×10^{16} m^{-2} under the *x*-polarized incident light, which correspond 34 to 170 V of $V_G - V_{CNP}$. However, the resonant wavelength obviously shifts as the gate voltage applied on graphene changes using *y*-polarized incident light. The resonant wavelength shifts by a significant amount of 0.52 μm, corresponding to 7.1% of the central operating wavelength of 7.36 μm. This distinct blue shift of wavelength is a result of the reduced capacitive coupling between neighboring apertures when graphene becomes more conductive as its carrier density increases.[27] In addition, the maximum tuning of phase is 180° at λ = 7.1 μm, which can be expanded by further increasing the gate voltage applied on graphene. Different tunable ranges along the *x*- and *y*-directions provide a convenient approach for adjusting the amplitude attenuation ratio r_{xy} and phase retardation difference δ. To quantitatively analyze the difference between illumination with *x*- and *y*-polarized incident light, Figure 1d shows the phase retardation difference δ as a function of wavelength, showing that δ can be widely tuned within the large wavelength range. The specific values of δ = 90°, 180°, and 270° can be obtained at 7.1 μm when the carrier density of graphene is 1.5×10^{16} m^{-2}, 3.9×10^{16} m^{-2}, and 7.5×10^{16} m^{-2}, which correspond to gate bias voltage 34, 89, and 170 V, respectively. These three values of δ correspond to the phase differences of light with RCP, linearly polarized (LP), and LCP light occurring between the two orthogonal E-field components, respectively. Moreover, these results provide a foundation for widely tuning the polarization state of the reflected light at 7.1 μm.

The different optical responses that occur as the gate voltage applied on graphene is changed under two orthogonally polarized incident light beams is ascribed to the anisotropy of

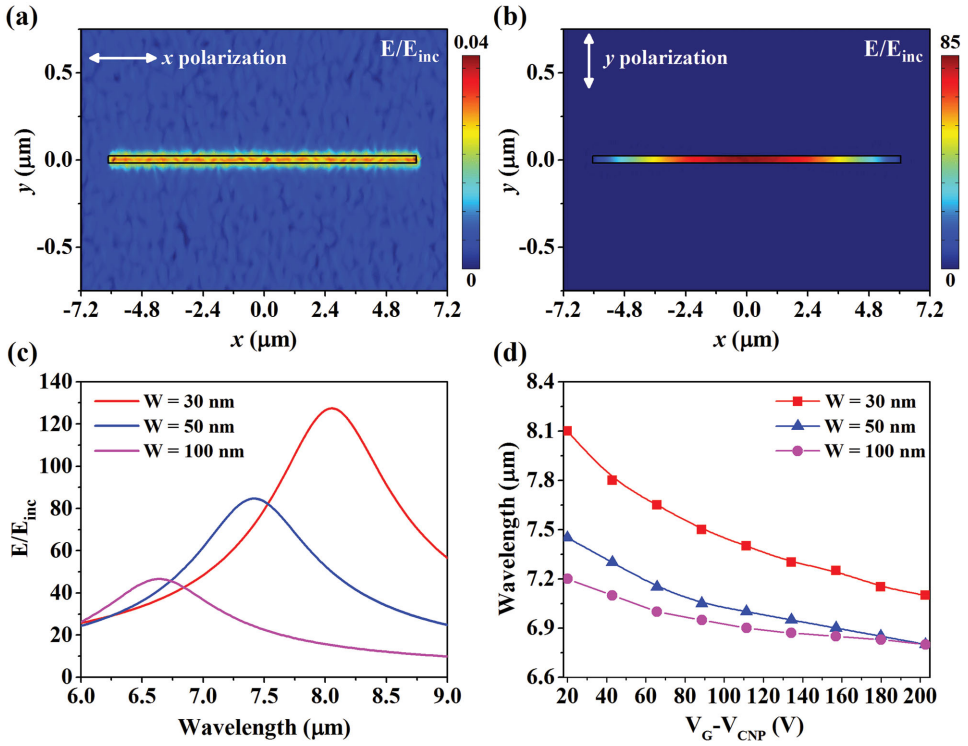

Figure 2. a,b) Calculated normalized near-field distribution within the plane at the location of graphene when illuminated with *x*- and *y*-polarized incident light, respectively. The wavelength of the incident light is 7.36 μm, which corresponds to the resonance peak with 20 V of gate voltage. c) Calculated normalized near-field intensity spectra for the rectangular nanoaperture with different width lengths *W* under *y*-polarized incident light when the gate voltage is 20 V. The near-field intensity spectra are plotted by the maximum normalized E-field intensity within the plane along the *z*-direction around graphene in the gap region at each wavelength. d) Resonance wavelength obtained from the rectangular nanoaperture with different width lengths *W* as a function of the gate voltage applied on graphene.

the rectangular nanoaperture, and this behavior is in good agreement with the theoretical predictions of Equation (2). **Figure 2**a,b show the normalized near-field spatial distributions of the rectangular nanoaperture under *x*- and *y*-polarized incident light, respectively, at the main resonant wavelength of 7.36 μm. The simulated results demonstrate that the light is hardly concentrated into the gap region when the incident polarization is parallel to the long side of rectangular nanoaperture because of the lack of surface plasmon polariton (SPP) resonance. Therefore, the intensity of electric field $\vec{E}$ around graphene in the gap region is very weak. The change of resonant frequency $\Delta\omega_{res}$ is nearly zero due to the small value of $\Delta\vec{\varepsilon}\cdot\vec{E}$ even though a large value of $\Delta\vec{\varepsilon}$ is obtained by changing the gate voltage applied on graphene. In contrast, when illuminated with *y*-polarized incident light, a strong E-field enhancement in the gap region and a distinct blue shift of the resonant wavelength can be obtained, as shown in Figure 2b, demonstrating that E-field enhancement by the metasurface plays an important role in the interaction between graphene and the metasurface. Moreover, this interaction offers an alternative way to tune $\Delta\omega_{res}$ through designing the geometrical parameter of the metasurface to generate different E-field enhancement intensities when maintaining $\Delta\vec{\varepsilon}$. Figure 2c shows the near-field intensity spectra of the rectangular nanoaperture with different width lengths under *y*-polarized incident light. The results demonstrate that the intensity of the E-field at the resonant wavelength distinctly decreases as the width length increases. In addition, when the gate voltage applied on graphene is changed from 20 to 205 V, the largest tunable range of $\Delta\omega_{res}$ corresponds to the case of W = 30 nm with maximum E-field intensity, as shown in Figure 2d. The tuning behavior agrees well with the relationship between $\Delta\omega_{res}$ and $\Delta\vec{\varepsilon}\cdot\vec{E}$ indicated in Equation (2). Therefore, the remarkable characteristics of the hybrid graphene metasurface can provide two independent degrees of freedom for controlling the tunable range of the amplitude and phase of light.

Taking advantage of the different optical responses in the *x*- and *y*-directions, wide modulation of the amplitude attenuation ratio r_{xy} and phase retardation difference δ can be realized within a large range of wavelengths. The specific amount of δ can reach 90° or 270° at 7.1 μm when the gate voltage applied on graphene is 34 or 170 V respectively, which offers a feasible method to transform the LP incident light into circularly polarized light. When illuminated with LP incident light, the Jones vector of the reflected light (Equation (1) shows that the generation of circularly polarized light requires not only the specific value of $\delta = 90°$ or 270° but also the same *E*-field intensities between two orthogonal components ($r_{xy}\cos\theta = \sin\theta$). In other words, the incident polarization direction should be set as $\arctan\left(r_{xy}\right)$ to satisfy this requirement. Considering the proposed metadevice, r_{xy} equals 1.8 when the gate voltage applied on graphene is 34 V or 170 V at the wavelength of 7.1 μm, which corresponds to the intersection of two reflection spectra curves, as shown in Figure 1c. Thus, the polarization direction of incident light is fixed at 61° relative to the *x*-axis. **Figure 3**b,c show the reflection spectra and normalized Stokes parameter S_3 as a function of

Adv. Optical Mater. **2015**,
DOI: 10.1002/adom.201500398

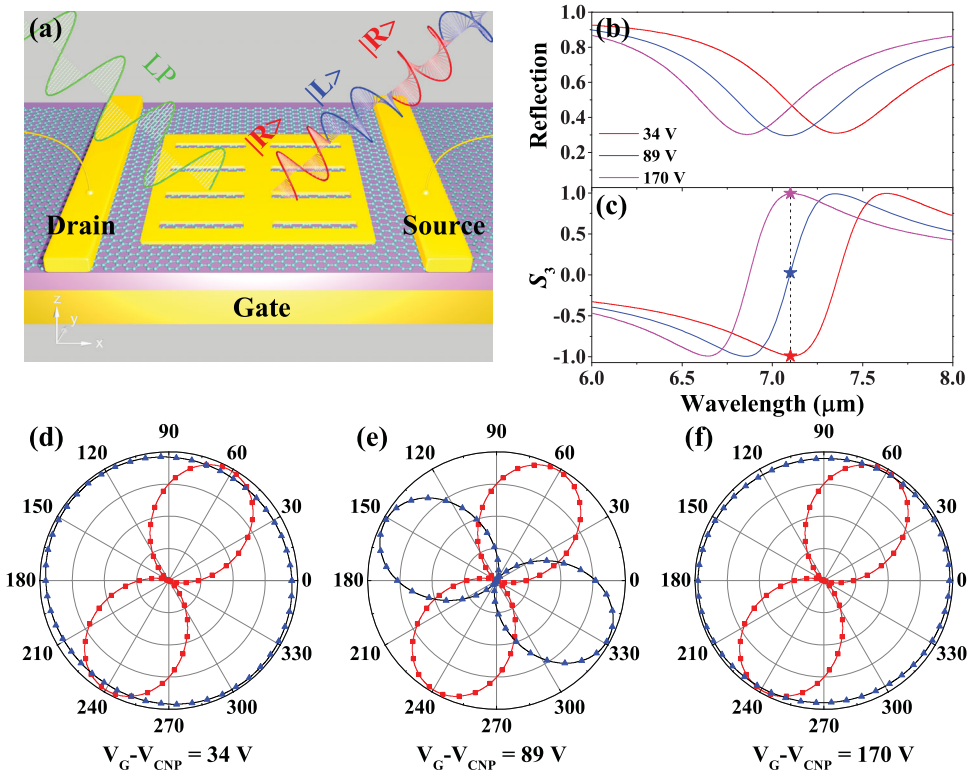

Figure 3. a) Schematic illustration of the optical polarization encoding process based on the circular orthogonal polarization basis. b,c) Simulated amplitude and normalized Stokes parameter S_3 spectra of the reflected light from the nanoaperture array at different gate voltages under incident light with a polarization direction of 61° relative to the *x*-axis. The stars indicate the values of S_3 under different gate voltages at 7.1 μm. d–f) Simulated polarization state in the plane perpendicular to the wave vector at 7.1 μm for different gate voltages. Red and blue curves correspond to the incident and reflected light, respectively.

the wavelength. A large reflection amplitude and widely tunable range of the polarization state can be obtained. As expected, the LP incident light can be transformed into ideal LCP or RCP light at 7.1 μm when the gate voltage applied on graphene is 34 or 170 V, respectively, as illustrated in Figure 3d, f. Moreover, S_3 of these two cases is nearly −1 and 1, respectively. The slight deviation from perfectly circularly polarized light can be resolved by optimizing the geometrical parameter and by improving the carrier density precision of graphene. When the gate voltage applied on graphene is 89 V, the amplitude attenuation ratio r_{xy} is 3.5, and the phase retardation difference δ is 180°. According to Equation (1), the Jones vector of the reflected light can be expressed as $\begin{bmatrix} -3.5\cos(61°) \\ \sin(61°) \end{bmatrix}$. Thus, the reflected light is linear polarized with a polarization direction of about 153°, which is nearly perpendicular to that of the incident light, as shown in Figure 3e. Therefore, the three fundamental polarizations of LCP, LP, and RCP light can be dynamically obtained by the proposed metadevice by switching the gate voltage applied on graphene among three different values at an incident wavelength of 7.1 μm. The proposed metadevice can be employed to realize the encoding of binary data based on light with circular orthogonal polarization basis. As shown in Figure 3a, the metadevice can be used to generate a special sequence of LCP and RCP light in the time domain, which correspond to the sequence of 0 and 1 in binary numeral system by switching the external voltage to dynamically tune the carrier density of graphene.

For more general cases, the proposed metadevice can offer more polarization states by continuously changing the gate voltage applied on graphene. As indicated in Figure 2c, the spectrum of Stokes parameter S_3 has an obvious blue shift as the gate voltage applied on graphene increases. Therefore, a large variation range of S_3 can be achieved at a fixed wavelength when the gate voltage is gradually increased from 20 to 205 V. **Figure 4**a illustrates three calculated normalized Stokes parameters as a function of the gate voltage when excited by an LP incident light with 61° polarization direction relative to the *x*-axis at a wavelength of 7.1 μm. The value of Stokes parameter S_3 varies within the range of −1 to 1, which represents the different polarization states. To clearly visualize the reflected light when the Stokes parameters vary, the corresponding polarization states have been plotted on the Poincaré sphere, as shown in Figure 4b. The variation of Stokes parameters forms a continuous path on the Poincaré sphere, starting near the South Pole and ending at the North Pole. This path represents continuous polarization evolution from LCP to RCP light as the gate voltage applied on graphene increases. Therefore, all polarization states on the path can be flexibly tuned by setting the corresponding the gate voltage, enabling the realization of encoding decimal or hexadecimal data using the polarization of light.

When illuminated with LP incident light at the wavelength of 7.1 μm, the polarization of the reflected light from the proposed hybrid graphene metasurface can be dynamically modulated into two orthogonal polarization states (LCP and RCP) and the

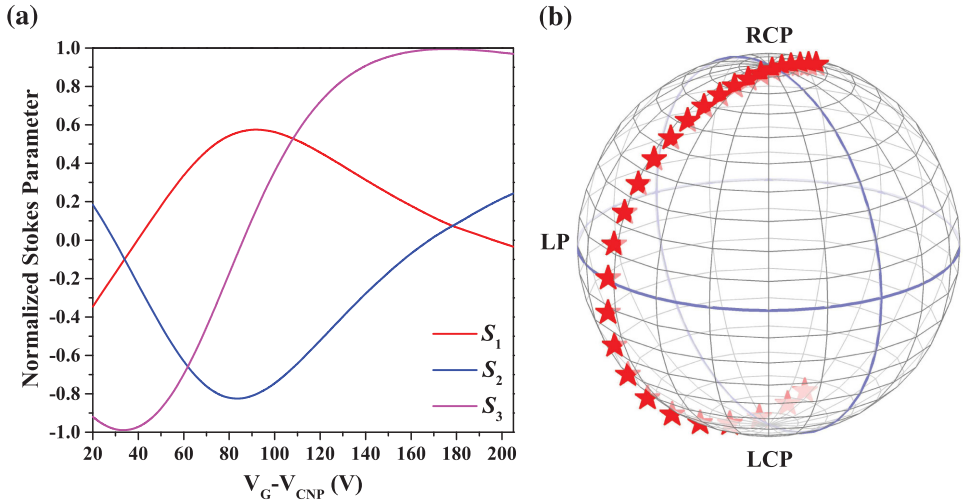

Figure 4. a) Normalized Stokes parameters as a function of the gate voltage applied on graphene. b) Corresponding polarization states (red stars) for different Stokes parameters on the Poincaré sphere.

corresponding superposition state (LP). Similarly, dynamical modulation to another two orthogonal polarization states (two perpendicular LP states) and their corresponding superposition state can also be realized when the specific value of $\delta = 90°$, 180°, and 270° is caused by the proposed structure. When the hybrid graphene metasurface is excited by the elliptically polarized light, whose Jones vector is $\begin{bmatrix} i\cos(61°) \\ \sin(61°) \end{bmatrix}$, the simulated Stokes parameter S_3 of the reflected light at 7.1 μm is 0 when the gate voltage applied on graphene is 34 or 170 V, as shown in **Figure 5**c. Thus, the reflected light is LP light for both cases. According to Equation (1), the Jones vector of the two reflected beams is $\begin{bmatrix} -1 \\ 1 \end{bmatrix}$ and $\begin{bmatrix} 1 \\ 1 \end{bmatrix}$, whose polarization directions are vertical with each other. The corresponding simulation results are shown in Figure 5d,f, and these results agree well with the theoretical calculations above.

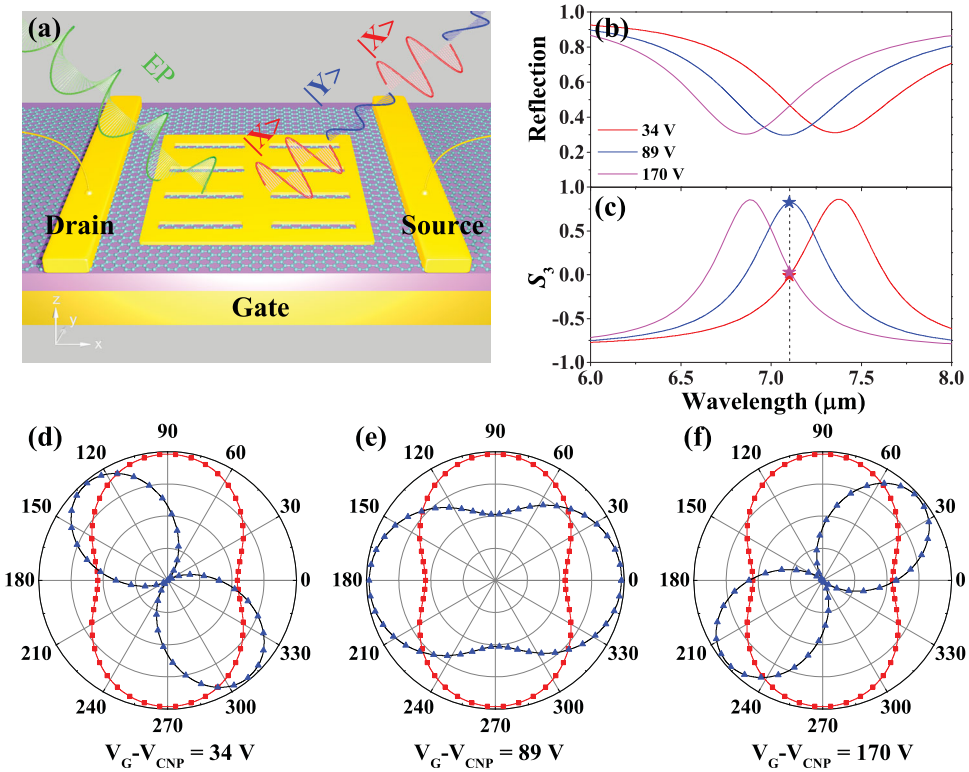

Figure 5. a) Schematic illustration of the optical polarization encoding process based on the linear orthogonal polarization basis. b,c) Simulated amplitude and normalized Stokes parameter S_3 spectra of the reflected light from the nanoaperture array at different gate voltages under incident light with elliptical polarization. The stars indicate the values of S_3 under different gate voltages at 7.1 μm. d–f) Simulated polarization state in the plane perpendicular to the wave vector at 7.1 μm for different gate voltages. Red and blue curves correspond to the incident and reflected light, respectively.

Adv. Optical Mater. **2015**,
DOI: 10.1002/adom.201500398

When the gate voltage is 89 V, the simulated and calculated results demonstrate that the reflected light is elliptically polarized light with same handedness as that of incident light. The main axis of the reflected light is about 153° relative to *x*-axis, which is nearly perpendicular to that of incident light, as shown in Figure 5e. This elliptically polarized reflected light can be regarded as the superposition state of two orthogonal polarization states $\begin{bmatrix} -1 \\ 1 \end{bmatrix}$ and $\begin{bmatrix} 1 \\ 1 \end{bmatrix}$. Similar to the circular orthogonal polarization basis (Figure 3a), polarization encoding based on the linear orthogonal polarization basis can also be achieved by the proposed metadevice when the illumination of EP light occurs as shown in Figure 5a.

As demonstrated above, the proposed metadevice can flexibly modulate the polarization state of the reflected light into two orthogonal polarization states as well as their superposition state by switching the gate voltage among three different values. Thus, the proposed metadevice can be used as multiplexer for realizing the PDM technique. As shown in **Figure 6**, two independent information signals can be, respectively, encoded into two orthogonally polarized light beams with a binary format. According to the superposition principle of polarization states, these two encoded light signals can be combined into a single light beam that has polarization modulation in the time domain. This light beam with a special polarization state sequence can be directly generated by the metadevice without requiring a coupling process for two light signals. In contrast, traditional PDM techniques generally require two optical paths for encoding two optical signals and a coupler for coupling these signals into a single physical channel. Therefore, the PDM technique can be simplified using the proposed metadevice.

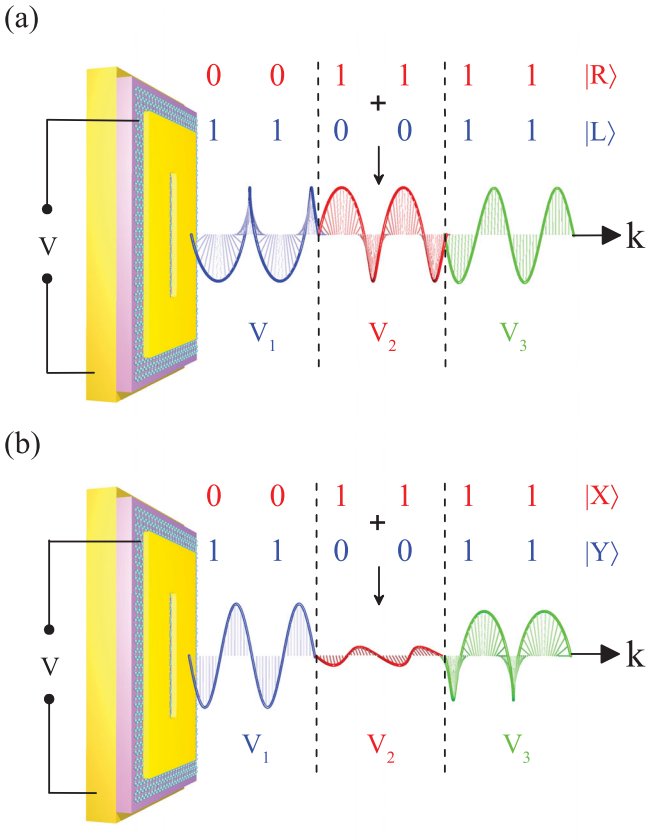

Figure 6. Schematic illustration of realizing the PDM technique by the proposed metadevice with the a) circular and b) linear orthogonal polarization basis according to the superposition principle of polarization states. Here, k and V indicate the wave vector and bias voltage, respectively. The three polarization states of light correspond to three difference gate voltages.

In the demultiplexing process, the polarization analyzer can be used to transfer a multiplexed light beam and recreate the original data stream. A recently reported metasurface has been regarded as an ideal demultiplexer, which is capable of generating different discontinuous interfacial phase profiles for two orthogonal polarization states. Such metasurfaces can decompose a light beam into two orthogonal polarized light beams along two different refraction directions.[47,48] Two independent information signals can be separated by such metasurfaces. Thus, the simple process of multiplexing and demultiplexing in the PDM technique can be accomplished using the metasurface-based devices with a compact volume.

In summary, we proposed a metadevice using a graphene-loaded metasurface, which can dynamically modulate the polarization state of light with a widely tunable range in MIR wavelengths. When the proposed metadevice is excited by LP light, the tunable polarization states of the reflected light can form a curve on the Poincaré sphere. This curve starts near the South Pole of the sphere and moves toward the North Pole as the gate voltage applied on graphene increases, representing a continuous polarization evolution from LCP to RCP light. The polarization state of the reflected light can be dynamically modulated into RCP, LCP, and LP light by changing the gate voltage among three different values. Moreover, when the polarization modulator is illuminated with EP light, two mutually perpendicularly LP lights and EP light can be generated in the reflection direction, corresponding to the three gate voltages. Based on the characteristics of polarization-control feature, we employ the metadevice for realizing polarization encoding based on linear and circular orthogonal polarization bases. Moreover, the concept of a metadevice-based PDM technique is demonstrated, which can double the transmission capacity in a single physical channel. The proposed metadevice can directly generate an optical beam with special polarization modulation, largely simplifying the process of multiplexing in the PDM technique. The resonant wavelength of graphene-loaded metasurface has an obvious red shift as increasing the thickness of the spacer layer illuminated by y-polarized incident light. The mechanism of dynamically modulating the polarization state can work in a large range of wavelength. Therefore, the ideal optical performance can also be obtained for other thicknesses of the spacer layer if other geometry parameters can be appropriately optimized. It has been demonstrated that the spectral tuning of graphene-loaded plasmonic metasurfaces has switching speeds up to 40 MHz, which is limited by the RC (circuit resistance × circuit capacitance) time constant of the biasing circuit.[27] This switching speed is much faster than that of dynamical tuning methods based on thermal, mechanical mechanisms. Although switching speeds of graphene-loaded plasmonic metasurfaces are lower than that of optical pump active metadevices (enabling THz-level switching speeds),[49–51]

it still fulfills the demand of faster information transfer and processing, and opens a route to on-chip integration of metasurfaces with electronics. By introducing new degrees of freedom for manipulating the light polarization state, this metadevice is expected to impact a wide range of photonic applications, ranging from optical communication to information encryption.

Acknowledgements

This work was supported by the National Basic Research Program (973 Program) of China (2012CB921900), the Chinese National Key Basic Research Special Fund (2011CB922003), the Natural Science Foundation of China (11574163, 61378006, and 11304163), the Program for New Century Excellent Talents in University (NCET-13-0294), the Natural Science Foundation of Tianjin (13JCQNJC01900), the International Science & Technology Cooperation Program of China (2013DFA51430), and 111 project (B07013).

Received: July 20, 2015
Revised: September 20, 2015
Published online:

[1] N. Yu, F. Capasso, *Nat. Mater.* **2014**, *13*, 139.
[2] A. Silva, F. Monticone, G. Castaldi, V. Galdi, A. Alu, N. Engheta, *Science* **2014**, *343*, 160.
[3] N. K. Grady, J. E. Heyes, D. R. Chowdhury, Y. Zeng, M. T. Reiten, A. K. Azad, A. J. Taylor, D. A. Dalvit, H. T. Chen, *Science* **2013**, *340*, 13047.
[4] N. Yu, F. Aieta, P. Genevet, M. A. Kats, Z. Gaburro, F. Capasso, *Nano Lett.* **2012**, *12*, 63283.
[5] H. Cheng, Z. Liu, S. Chen, J. Tian, *Adv. Mater.* **2015**, *27*, 5410.
[6] N. Yu, P. Genevet, M. A. Kats, F. Aieta, J.-P. Tetienne, F. Capasso, Z. Gaburro, *Science* **2011**, *334*, 333.
[7] S. Sun, K. Y. Yang, C. M. Wang, T. K. Juan, W. T. Chen, C. Y. Liao, Q. He, S. Xiao, W. T. Kung, G. Y. Guo, L. Zhou, D. P. Tsai, *Nano Lett.* **2012**, *12*, 62239.
[8] C. Pfeiffer, N. K. Emani, A. M. Shaltout, A. Boltasseva, V. M. Shalaev, A. Grbic, *Nano Lett.* **2014**, *14*, 24917.
[9] J. Li, S. Chen, H. Yang, J. Li, P. Yu, H. Cheng, C. Gu, H.-T. Chen, J. Tian, *Adv. Funct. Mater.* **2015**, *25*, 704.
[10] H. Cheng, S. Chen, P. Yu, W. Liu, Z. Li, J. Li, B. Xie, J. Tian, *Adv. Opt. Mater.* **2015**, DOI: 10.1002/adom.2015000285.
[11] X. Yin, Z. Ye, J. Rho, Y. Wang, X Zhang, *Science* **2013**, *339*, 14057.
[12] N. Liu, M. Mesch, T. Weiss, M. Hentschel, H Giessen, *Nano Lett.* **2010**, *10*, 23428.
[13] N. I. Landy, S. Sajuyigbe, J. J. Mock, D. R. Smith, W. J. Padilla, *Phys. Rev. Lett.* **2008**, *100*, 207402.
[14] S. Chen, H. Cheng, H. Yang, J. Li, X. Duan, C. Gu, J. Tian, *Appl. Phys. Lett.* **2011**, *99*, 253104.
[15] Y. Zhao, M. A. Belkin, A. Alu, *Nat. Commun.* **2012**, *3*, 870.
[16] H. Cheng, S. Chen, P. Yu, J. Li, B. Xie, Z. Li, J. Tian, *Appl. Phys. Lett.* **2013**, *103*, 223012.
[17] H. Cheng, S. Chen, P. Yu, J. Li, L. Deng, J. Tian, *Opt. Lett.* **2013**, *38*, 1567.
[18] O. Y. Yermakov, A. I. Ovcharenko, M. Song, A. A. Bogdanov, I. V. Iorsh, Y. S. Kivshar, *Phys. Rev. B* **2015**, *91*, 235423.
[19] N. I. Zheludev, Y. S. Kivshar, *Nat. Mater.* **2012**, *11*, 917.
[20] N. I. Zheludev, *Science* **2015**, *348*, 973.
[21] J. Y. Ou, E. Plum, L. Jiang, N. I. Zheludev, *Nano Lett.* **2011**, *11*, 2142.
[22] M. Lapine, I. V. Shadrivov, D. A. Powell, Y. S. Kivshar, *Nat. Mater.* **2012**, *11*, 30.
[23] J. Zhang, K. F. MacDonald, N. I. Zheludev, *Phys. Rev. B* **2012**, *85*, 205123.
[24] F. H. L. Koppens, D. E. Chang, F. J. García de Abajo, *Nano Lett.* **2011**, *11*, 3370.
[25] J. Chen, M. Badioli, P. Alonso-Gonzalez, S. Thongrattanasiri, F. Huth, J. Osmond, M. Spasenovic, A. Centeno, A. Pesquera, P. Godignon, A. Z. Elorza, N. Camara, F. J. G. de Abajo, R. Hillenbrand, F. H. L. Koppens, *Nature* **2012**, *487*, 77.
[26] H. Cheng, S. Chen, P. Yu, X. Duan, B. Xie, J. Tian, *Appl. Phys. Lett.* **2013**, *103*, 203112.
[27] Y. Yao, M. A. Kats, P. Genevet, N. Yu, Y. Song, J. Kong, F. Capasso, *Nano Lett.* **2013**, *13*, 1257.
[28] Z. Fang, Z. Liu, Y. Wang, P. M. Ajayan, P. Nordlander, N. J. Halas, *Nano Lett.* **2012**, *12*, 3808.
[29] F. Valmorra, G. Scalari, C. Maissen, W. Fu, C. Schonenberger, J. W. Choi, H. G. Park, M. Beck, J. Faist, *Nano Lett.* **2013**, *13*, 3193.
[30] Q. Li, Z. Tian, X. Zhang, R. Singh, L. Du, J. Gu, J. Han, W. Zhang, *Nat. Commun.* **2015**, *6*, 7082.
[31] Q. Li, Z. Tian, X. Zhang, N. Xu, R. Singh, J. Gu, P. Lv, L.-B. Luo, S. Zhang, J. Han, W. Zhang, *Carbon* **2015**, *90*, 146.
[32] S. H. Lee, M. Choi, T.-T. Kim, S. Lee, M. Liu, X. Yin, H. K. Choi, S. S. Lee, C.-G. Choi, S.-Y. Choi, X. Zhang, B. Min, *Nat. Mater.* **2012**, *11*, 936.
[33] N. Dabidian, I. Kholmanov, A. B. Khanikaev, K. Tatar, S. Trendafilov, S. H. Mousavi, C. Magnuson, R. S. Ruoff, G. Shvets, *ACS Photonics* **2015**, *2*, 216.
[34] X. Dou, H. Yin, H. Yue, Y. Jin, *Appl. Opt.* **2015**, *54*, 4509.
[35] A. Roberts, L. Lin, *Opt. Lett.* **2012**, *37*, 1820.
[36] Y. Zhao, A. Alu, *Nano Lett.* **2013**, *13*, 1086.
[37] J. Yang, J. Zhang, *Plasmonics* **2011**, *6*, 251.
[38] Y. Ye, S. He, *Appl. Phys. Lett.* **2010**, *96*, 203501.
[39] F. Wang, A. Chakrabarty, F. Minkowski, K. Sun, Q.-H. Wei, *Appl. Phys. Lett.* **2012**, *101*, 023101.
[40] K. S. Novoselov, A. K. Geim, S. V. Morozov, D. Jiang, Y. Zhang, S. V. Dubonos, I. V. Grigorieva, A. A. Firsov, *Science* **2004**, *306*, 666.
[41] J. A. Kong, *Electromagnetic Wave Theory,* EMW Publishing, Cambridge **2000**.
[42] Z. Li, N. Yu, *Appl. Phys. Lett.* **2013**, *102*, 131108.
[43] *COMSOL Multiphysics User's Guide, Version 3.5*, Comsol AB, Burlington, MA **2008**.
[44] E. D. Palik, *Handbook of Optical Constants of Solids,* Academic Press, New York **1998**.
[45] L. A. Falkovsky, S. S. Pershoguba, *Phys. Rev. B* **2007**, *76*, 153410.
[46] N. Petrone, C. R. Dean, I. Meric, A. M. van der Zande, P. Y. Huang, L. Wang, D. Muller, K. L. Shepard, J. Hone, *Nano Lett.* **2012**, *12*, 2751.
[47] M. Farmahini-Farahani, H. Mosallaei, *Opt. Lett.* **2013**, *38*, 462.
[48] D. Wen, F. Yue, S. Kumar, Y. Ma, M. Chen, X. Ren, P. E. Kremer, B. D. Gerardot, M. R. Taghizadeh, G. S. Buller, X. Chen, *Opt. Express* **2015**, *23*, 10272.
[49] R. Singh, J. Xiong, A. K. Azad, H. Yang, S. A. Trugman, Q. X. Jia, A. J. Taylor, H.-T. Chen, *Nanophotonics* **2012**, *1*, 117.
[50] J. Gu, R. Singh, A. K. Azad, J. Han, A. J. Taylor, J. F. O'Hara, W. Zhang, *Opt. Mater. Express* **2012**, *2*, 31.
[51] D. R. Chowdhury, R. Singh, A. J. Taylor, H.-T. Chen, A. K. Azad, *Appl. Phys. Lett.* **2013**, *102*, 011122.